


Article

The Effects of Metalloid Elements on the Nanocrystallization Behavior and Soft Magnetic Properties of FeCBSiPCu Amorphous Alloys

Zhichao Lu ¹ , Hongxiang Li ¹, Zhifeng Lei ¹, Chuntao Chang ², Xianzhen Wang ³ and Zhaoping Lu ^{1,*}

¹ State Key Laboratory for Advanced Metals and Materials, University of Science and Technology Beijing, Beijing 100083, China; lvzhichaodaniel@163.com (Z.Lu); hqli@skl.ustb.edu.cn (H.L.); zfleil@xs.ustb.edu.cn (Z.Lei)

² School of Mechanical Engineering, Dongguan University of Technology, Dongguan 523808, China; changct@dgut.edu.cn

³ Institute for Advanced Materials and Technology, University of Science and Technology Beijing, Beijing 100083, China; xzwang@163.com

* Correspondence: luzp@ustb.edu.cn; Tel.: +86-10-8237-5387

Received: 23 March 2018; Accepted: 17 April 2018; Published: 19 April 2018



Abstract: Soft magnetic properties of Fe-based metallic glasses (MGs) are dependent on their nanocrystallization behavior, particularly the precipitation of α -Fe embedded in the amorphous matrix. In this study, the effects of metalloid elements of C, B, Si, and P on thermal stability, nanocrystallization behavior, and soft magnetic properties of typical Fe-based amorphous alloys, i.e., the Fe-Cu-(CBSiP) glassy alloys, were investigated systematically. It is found that the addition of the metalloid elements can effectively retard the precipitation process of α -Fe during reheating of the Fe-based MGs due to the long-range diffusion of the metalloids; however, their individual effects on the compositional portioning and formation of other crystalline phases are varied. To achieve desirable soft magnetic properties, a species of metalloids and their concentrations have to be carefully controlled so that the formation of α -Fe does not interfere with that of other crystalline phases, especially those hard-magnetic phases.

Keywords: metalloid elements; nanocrystallization behavior; soft magnetic properties; Fe-based metallic glasses

1. Introduction

Fe-based metallic glasses (MGs) have attracted extensive attention due to their unique combination of good mechanical and soft magnetic properties [1–5]. Currently, a variety of soft magnetic Fe-based amorphous alloys and their composites have been developed, such as METGLAS, FINEMET, NANOPERM, HITPERM, and NANOMET [6–10]. Some of them have been widely using in transformer, motor, sensor, and other electric and electronic parts [11–15]. By proper annealing of these Fe-based metallic glasses, nanocrystallization of α -Fe would occur, resulting in a composite structure consisting of ultrafine grains homogeneously distributed in amorphous matrix. The coupling effect between α -Fe particles and the amorphous matrix, and the release of residual stress generated during preparation, tend to lead to better magnetic properties, including higher saturation magnetization M_S and lower coercivity H_C . It was reported that to achieve desirable soft magnetic properties, the following aspects should be taken into account:

1. Primary nanocrystallization of α -Fe has to be carefully controlled. In general, small sizes, high density, and homogenous distribution of α -Fe are beneficial for achieving large magnetization. In other words, nucleation of α -Fe should be stimulated, while its growth rate should be retarded.
2. Annealing usually tends to embrittle Fe-based MGs; the higher the annealing temperature, the more brittle the MGs would become. Therefore, precipitation of α -Fe at low temperatures is beneficial and preferred.
3. The stability of the residual amorphous matrix should be insufficiently high so that the formation of hard magnetic phases such as $\text{Fe}_3(\text{B,C,P})$ can be avoided.

As elaborated above, as far as soft magnetic properties are considered, the thermal stability of both the α -Fe primary phase and the remaining amorphous matrix have to be controlled, which is closely related to the types of metalloid constituents and their total concentration in Fe-based MGs. From a standpoint of glass-forming ability (GFA), nevertheless, α -Fe precipitation needs to be retarded during undercooling, which somewhat conflicts with the requirements for obtaining decent soft magnetic properties. To solve this dilemma and manipulate primary crystallization of α -Fe, effects of metalloids including C, B, Si, and P on thermal stability and soft magnetic properties of Fe-based MGs have to be investigated in detail. Currently, no consensus in this regard has been reached, and some experimental findings even contradict each other. For example, by studying FINEMET alloy, Kim et al. reported that the addition of P increased the primary crystallization temperature and coarsened the grain size, which led to the increased coercivity [16]. However, Cui et al. found the grain size dramatically decreased from 200 to about 20 nm with addition of 4 at. % P to FeSiB alloy [17]. For the metalloid element Si, it was also noted that by Si substituting P, the GFA was increased in $\text{Fe}_{70}\text{Al}_5\text{Ga}_2\text{P}_{12.65-x}\text{C}_{5.75}\text{B}_{4.6}\text{Si}_x$ alloys but decreased in $\text{Fe}_{83}\text{P}_{16-x}\text{Si}_x\text{Cu}_1$ alloys [18,19]. Moreover, effects of B and C are also not well understood; in many alloy systems such as (Fe, Cr)-metalloid (metalloid = C, B, or P) [20] and FePCB [21], B and C are effective at improving GFA. Nevertheless, it was reported that the increase of B in Fe-Zr-B amorphous alloys gave rise to the decrease of structural homogeneity in the bcc (body-centered-cubic) phase, resulting in the deterioration of soft magnetic properties [22].

In our previous work, an interesting series of FeCBSiPCu BMGs with high GFA and excellent soft magnetic properties [23] was developed. Unfortunately, formation of α -Fe overlapped with crystallization event of the residual amorphous matrix [i.e., formation of hard magnetic phase $\text{Fe}_3(\text{B,C,P})$]. Consequently, it is hard to obtain a uniform distribution of nanosized α -Fe particles without the formation of hard magnetic phases, which dramatically increase coercivity. In this paper, $\text{Fe}_{79.3}\text{C}_{3.1}\text{B}_{6.9}\text{Si}_{2.7}\text{P}_{7.3}\text{Cu}_{0.7}$ MG with a high Fe content was selected as a base alloy with which to scrutinize the effects of the metalloids on thermal stability and soft magnetic properties. The findings not only shed new insights into understanding nanocrystallization in amorphous solids, but also provide a useful guideline for developing novel soft magnetic amorphous alloys with a much wider annealing process window and better overall properties.

2. Materials and Methods

All alloy ingots with nominal compositions of $\text{Fe}_{77.3+x}\text{C}_{5.1-x}\text{B}_{6.9}\text{Si}_{2.7}\text{P}_{7.3}\text{Cu}_{0.7}$, $\text{Fe}_{77.3+x}\text{C}_{3.1}\text{B}_{8.9-x}\text{Si}_{2.7}\text{P}_{7.3}\text{Cu}_{0.7}$, $\text{Fe}_{77.3+x}\text{C}_{3.1}\text{B}_{6.9}\text{Si}_{4.7-x}\text{P}_{7.3}\text{Cu}_{0.7}$, and $\text{Fe}_{77.3+x}\text{C}_{3.1}\text{B}_{6.9}\text{Si}_{2.7}\text{P}_{9.3-x}\text{Cu}_{0.7}$ ($X = 0, 1, 2, 3$, and 4 at. %) were prepared by arc-melting mixtures of Fe (99.99 wt. %), Si (99.99 wt. %), B (99.9 wt. %), Cu (99.99 wt. %), and industrial Fe-P master alloys (P: 24.81, Si: 1.4, C: 0.028, S: 0.034, Cr: 0.14, Mn: 2.24, Ti: 1.37, B: 0.0075, Al: 0.21, wt. %) in a high purity argon atmosphere. Amorphous ribbons, typically 1–1.5 mm wide and 25–30 μm thick, were produced by the melt-spinning technique with a surface speed of 40 m/s.

Thermal properties of all as-spun amorphous ribbons were evaluated using differential scanning calorimetry (DSC) at a heating rate of 0.33 K/s with argon as purging gas. According to the corresponding DSC curves, the amorphous specimens were annealed at different temperatures for 600 s under argon atmosphere. Microstructures of the as-spun and annealed ribbons were identified

by X-ray diffraction (XRD) with Cu K α radiation. Some ribbons with representative compositions and magnetic properties were further investigated by transmission electron microscopy (TEM). The M_s values of all the as-spun and some annealed ribbons were characterized with a vibrating sample magnetometer (VSM) under an applied field of -800 to 800 kA/m. Coercivity (H_C) was measured by using a B–H loop tracer under a field of 1000 A/m.

3. Results and Discussion

3.1. Thermal Stability

XRD patterns for all as-spun ribbon samples are shown in Figure 1. Clearly, all specimens exhibit a diffuse peak, indicative of their fully amorphous nature. Figure 2 demonstrates the corresponding DSC curves of these as-prepared Fe-based MGs at a heating rate of 0.33 K/s. Similar crystallization behavior showing two main exothermic peaks was observed for all the selected compositions. T_C , T_{x1} , and T_{x2} correspond to Curie temperature, and crystallization temperature of the 1st and 2nd peak, respectively. All the related thermal stability parameters are summarized in Table 1.

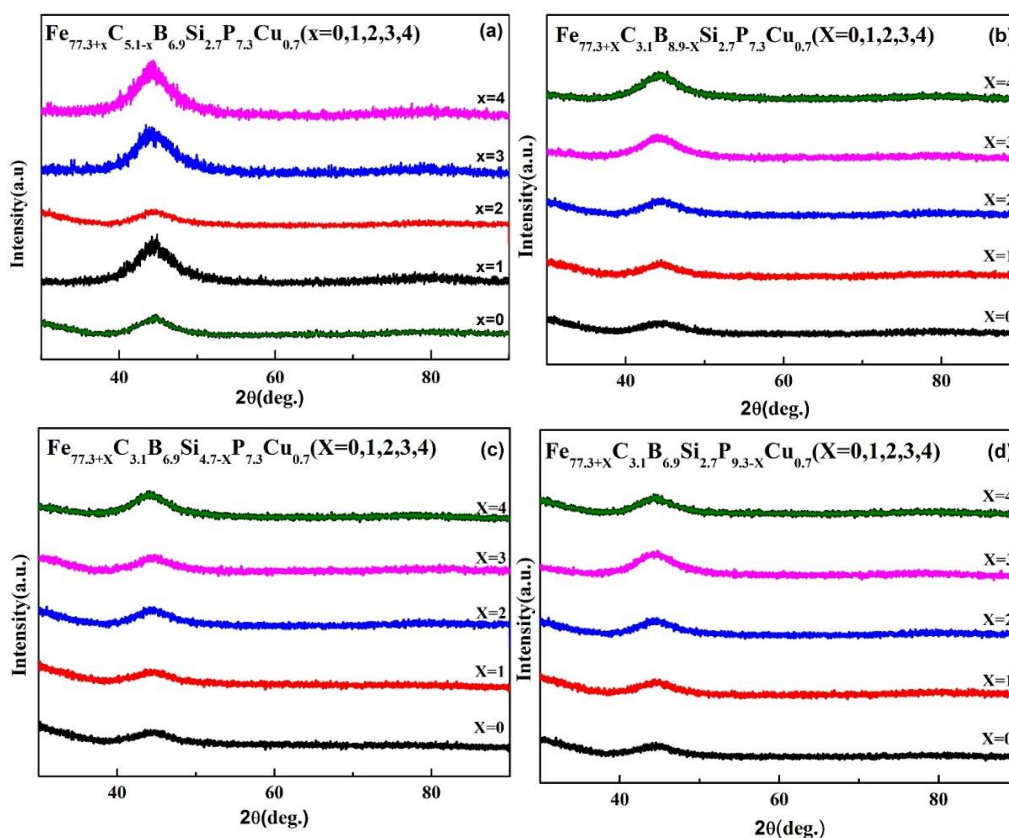


Figure 1. XRD patterns of as-prepared FeCBSiPCu MGs.

As can be seen from Figure 2a, with the increase of the C content, the first peak shifts gradually toward higher temperatures, while the second peak keeps almost unchanged. The first peak temperature (T_{x1}) and the second peak temperature (T_{x2}) as a function of C content are listed in Table 1. As demonstrated in Figure 2b, the addition of B in these alloys has similar effects on their crystallization behavior, i.e., the first peak temperature shifts toward higher temperatures, while the second peak position is the same. All these observations reveal that increasing the content of either C or B can appreciably suppress the precipitation of primary phase during annealing process but has little impact on the crystallization of residual amorphous phase.

The influence of Si addition on the crystallization behavior of the current Fe-based MGs is presented in Figure 2c. From the DSC curves, it is known that increasing the Si content shifts both crystallization peaks to higher temperatures, but rise of the first peak temperature is much larger than the second peak temperature (see Table 1 as well). These results uncover that increasing Si in the alloys could retard both crystallization stages, but is more pronounced on the crystallization of primary phase.

Figure 2d displays effects of P on the crystallization behavior of Fe-based MGs. Surprisingly, the two exothermic peaks move closer as the P content is raised. As also tabulated in Table 1, when P increases from 5.3 to 9.3 at. %, the first peak temperature T_{x1} increases from 697 to 760 K, while the second peak temperature T_{x2} decreases from 807 to 785 K. It is clear that addition of P could retard the crystallization of primary phase but destabilizes the residual amorphous phase.

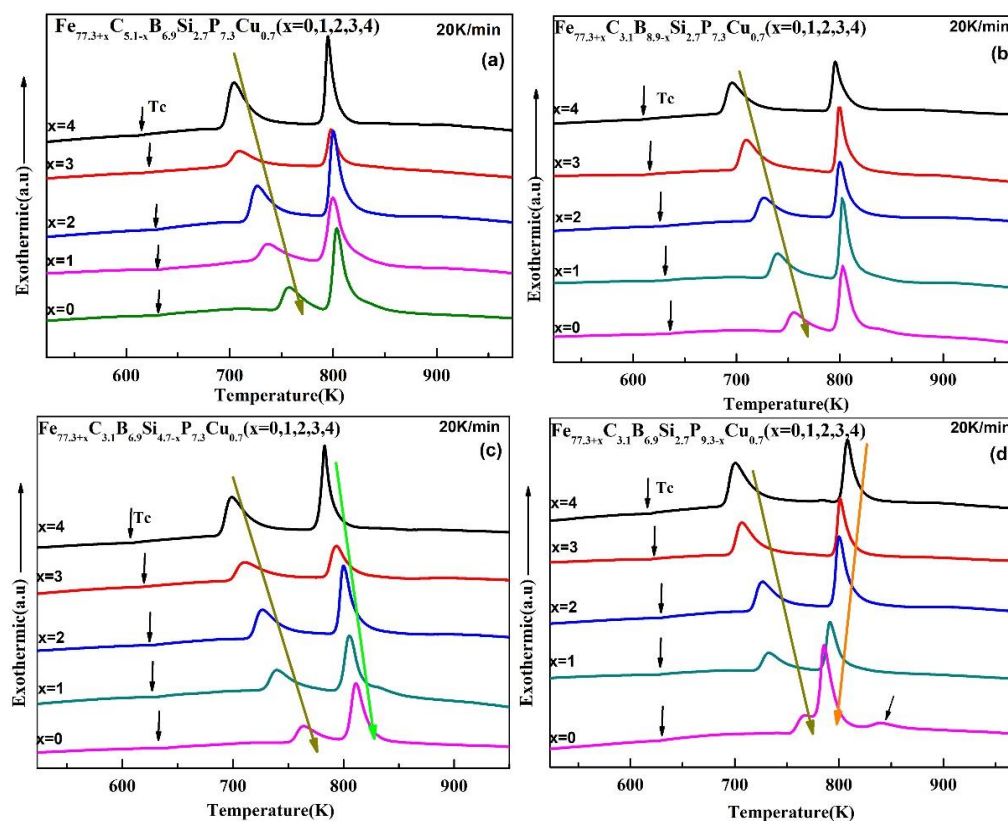


Figure 2. DSC curves of as-prepared FeCBSiPCu MGs at a heating rate of 0.33 K/s.

As shown in Table 1, $\text{Fe}_{81.3}\text{C}_{3.1}\text{B}_{4.9}\text{Si}_{2.7}\text{P}_{7.3}\text{Cu}_{0.7}$ alloy has the largest ΔT_x —($T_{x2} - T_{x1}$) of 108 K among all the alloys investigated, which provides the widest annealing window for subsequent heat treatment. Thus, it is much easier to control the precipitation of α -Fe and $\text{Fe}_3\text{P}(\text{C}, \text{B})$ by annealing in such a wider temperature range. To investigate detailed crystallization process associated with these exothermic events, TEM characterization of the specimens annealed at certain temperatures for 10 mins, i.e., the temperature after the 1st and 2nd peak were conducted for as-spun ribbons. As an example, Figure 3 shows the bright-field TEM images, selected area electron diffraction (SAED) patterns, and high resolution microstructures for $\text{Fe}_{81.3}\text{C}_{3.1}\text{B}_{4.9}\text{Si}_{2.7}\text{P}_{7.3}\text{Cu}_{0.7}$ alloys of as-cast and annealed at different temperatures. Figure 3b shows that nano-scale α -Fe grains embedded in residual amorphous matrix uniformly for $\text{Fe}_{81.3}\text{C}_{3.1}\text{B}_{4.9}\text{Si}_{2.7}\text{P}_{7.3}\text{Cu}_{0.7}$ alloy annealed at 743 K for 10 min, which corresponds to the SAED pattern consisting of both a diffused halo ring pattern produced by residual amorphous matrix and distinct spot rings generated by the nanocrystalline α -Fe. Figure 3c–e shows the SAED pattern and high resolution microstructures for $\text{Fe}_{81.3}\text{C}_{3.1}\text{B}_{4.9}\text{Si}_{2.7}\text{P}_{7.3}\text{Cu}_{0.7}$ alloy annealed at 843 K for

10 min. It can be seen clearly that complex phase forms in residual amorphous matrix. According to the high resolution microstructures, the new phase is $\text{Fe}_3\text{P}(\text{C,B})$, which is consistent with the XRD results. So T_{x2} corresponds to the formation of phosphorus-enriched phase $\text{Fe}_3\text{P}(\text{C,B})$.

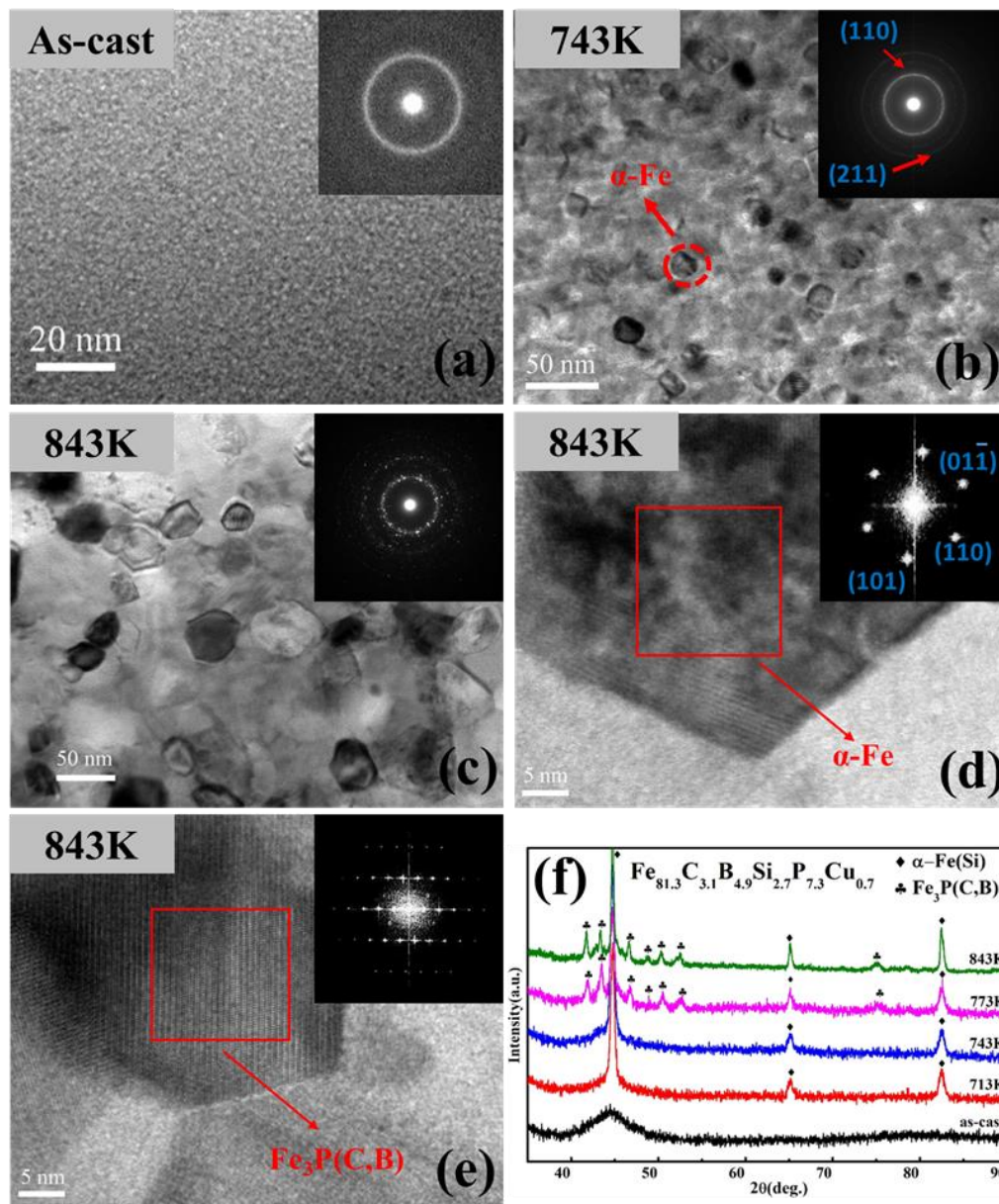


Figure 3. TEM images for $\text{Fe}_{81.3}\text{C}_{3.1}\text{B}_{4.9}\text{Si}_{2.7}\text{P}_{7.3}\text{Cu}_{0.7}$ alloys of as-cast (a), annealed at 743 K (b), and annealed at 843 K (c) for 10 min; HRTEM images for $\text{Fe}_{81.3}\text{C}_{3.1}\text{B}_{4.9}\text{Si}_{2.7}\text{P}_{7.3}\text{Cu}_{0.7}$ alloy annealed at 843 K for 10 min (d,e) and XRD patterns of $\text{Fe}_{81.3}\text{C}_{3.1}\text{B}_{4.9}\text{Si}_{2.7}\text{P}_{7.3}\text{Cu}_{0.7}$ alloy as-cast and annealed at different temperatures (f).

As elaborated above, the first crystallization peak corresponds to precipitation of the $\alpha\text{-Fe}$ phase, while the second at higher temperatures related to crystallization event of the remaining amorphous phase can be confirmed by TEM characterization shown in Figure 3. Based on the above experimental data, adjusting the type or/and concentration of metalloid elements could manipulate crystallization behavior of Fe-based MGs so that desirable characteristics of $\alpha\text{-Fe}$ particles and a wide annealing process window (i.e., the temperature span between the two crystallization peaks) can be achieved. It is clear that addition of all the metalloid elements investigated, i.e., P, C, B, and Si, can effectively retard

the precipitation process of α -Fe during reheating of the Fe-based MGs. According to phase diagrams, the solid solution limit of α -Fe with C, B, Si, and P is 0.1, 0, 19.6, and 4.9 at. %, respectively. Thus, during the primary crystallization of α -Fe, long-range diffusion of the metalloids is necessary because of their limited solubility in Fe. Rejection of these metalloids suppresses formation of α -Fe, shifting the crystallization event to higher temperature remarkably, i.e., increasing the T_{x1} value. In general, glass formation is virtually to avoid formation of any crystalline phases; suppression of α -Fe would usually result in large GFA.

As revealed in Figure 3, this late crystallization stage is mainly related to formation of $\text{Fe}_3\text{P}(\text{C}, \text{B})$. Note that, according to Miedema's theory [24], formation enthalpy of Fe_3C , Fe_3B , Fe_3Si , and Fe_3P were calculated to be -1.4 , -23 , -21 , and -50 kJ/mol, respectively. The estimated standard formation enthalpy of Fe_3P is much larger than that of Fe_3C , Fe_3B , and Fe_3Si , suggesting that Fe_3P can form much easier than Fe_3C , Fe_3B , and Fe_3Si . Therefore, phosphorus-enriched phase tends to be formed with the solution of other metalloids like C, B, and Si. As phosphorus-enriched phase is formed easier than the other three phases, so T_{x2} is mainly affected by formation of this phase. Thus, as presented by Figure 2, decreasing carbon content leads to few changes of T_{x2} . The invariant of T_{x2} results from the constant level of P content. Namely, decreasing carbon content has nearly no remarkable influence on the precipitation of phosphorus-enriched phase. Additionally, increasing boron content is similar to that of C. However, influence of Si on T_{x2} of all alloys is different: for the increasing of Si content, the T_{x2} moves to higher temperature. Part of Si is solute in α -Fe, with rest of it remaining in residual amorphous matrix. Thus, by increasing Si content, residual amorphous matrix could be more stable and leads T_{x2} to higher temperature. Effects of P on thermal stability are different from those of other metalloids. According to Fe-P phase diagram, it can be seen that the liquidus tend to move to lower temperature by increasing P content, which leads to the process of crystalline changing from hypoeutectic type to eutectic type consistent with DSC results.

Table 1. Thermal stability and magntic properties of FeCBSiPCu MGs.

Alloys	X	Thermal Stability			Soft Magnetic Properties		
		T_{x1} (K)	T_{x2} (K)	ΔT_x (K)	M_s (T)	T_C (K)	H_C (A/m)
$\text{Fe}_{77.3+x}\text{C}_{5.1-x}\text{B}_{6.9}\text{Si}_{2.7}\text{P}_{7.3}\text{Cu}_{0.7}$	0	746	795	49	1.45	630	9.8
	1	726	792	66		631	8.0
	2	709	791	82	1.51	628	11.1
	3	698	793	95		621	15.9
	4	691	788	97	1.58	610	21.4
$\text{Fe}_{77.3+x}\text{C}_{3.1}\text{B}_{8.9-x}\text{Si}_{2.7}\text{P}_{7.3}\text{Cu}_{0.7}$	0	745	793	48	1.43	632	11.0
	1	729	794	65		631	5.8
	2	709	791	82	1.51	628	11.1
	3	699	793	94		610	12.0
	4	683	791	108	1.63	601	20.2
$\text{Fe}_{77.3+x}\text{C}_{3.1}\text{B}_{6.9}\text{Si}_{4.7-x}\text{P}_{7.3}\text{Cu}_{0.7}$	0	752	802	50	1.40	638	11.5
	1	728	796	68		634	26.2
	2	709	791	82	1.51	628	11.1
	3	696	781	85		620	8.4
	4	682	773	91	1.55	608	7.3
$\text{Fe}_{77.3+x}\text{C}_{3.1}\text{B}_{6.9}\text{Si}_{2.7}\text{P}_{9.3-x}\text{Cu}_{0.7}$	0	746	774	28	1.43	628	5.4
	1	721	783	62		628	8.2
	2	709	791	82	1.51	628	11.1
	3	696	795	99		618	8.6
	4	686	799	82	1.61	618	23.4

3.2. Soft Magnetic Properties

Figure 4a shows the M_s measured with VSM of $\text{Fe}_{77.3+x}\text{C}_{5.1-x}\text{B}_{6.9}\text{Si}_{2.7}\text{P}_{7.3}\text{Cu}_{0.7}$, $\text{Fe}_{77.3+x}\text{C}_{3.1}\text{B}_{8.9-x}\text{Si}_{2.7}\text{P}_{7.3}\text{Cu}_{0.7}$, $\text{Fe}_{77.3+x}\text{C}_{3.1}\text{B}_{6.9}\text{Si}_{4.7-x}\text{P}_{7.3}\text{Cu}_{0.7}$, and $\text{Fe}_{77.3+x}\text{C}_{3.1}\text{B}_{6.9}\text{Si}_{2.7}\text{P}_{9.3-x}\text{Cu}_{0.7}$ ($X = 0, 2$ and 4) amorphous as-spun ribbons, respectively. When the content of metalloid elements

is decreased, M_S has an increasing trend for all as-prepared ribbons. Specifically, the M_S increases gradually from 1.45 T to 1.58 T, 1.43 T to 1.63 T, 1.40 T to 1.55 T, and 1.43 T to 1.61 T when the content of C, B, Si and P is decreased. Due to the large negative mixing heat between Fe and metalloid elements, the addition of metalloid elements tends to generate Fe-metalloid atomic pairs. It should consider the electron interactions of Fe and metalloid elements. For C, B, Si, P elements, which all have p electrons, the p orbitals interact with 3d electrons of Fe, which would lead to the reduction of the effective magneton number. As a result, with the addition of metalloid elements, the saturated magnetization tends to be decreased, which is consistent with previous work [16,22].

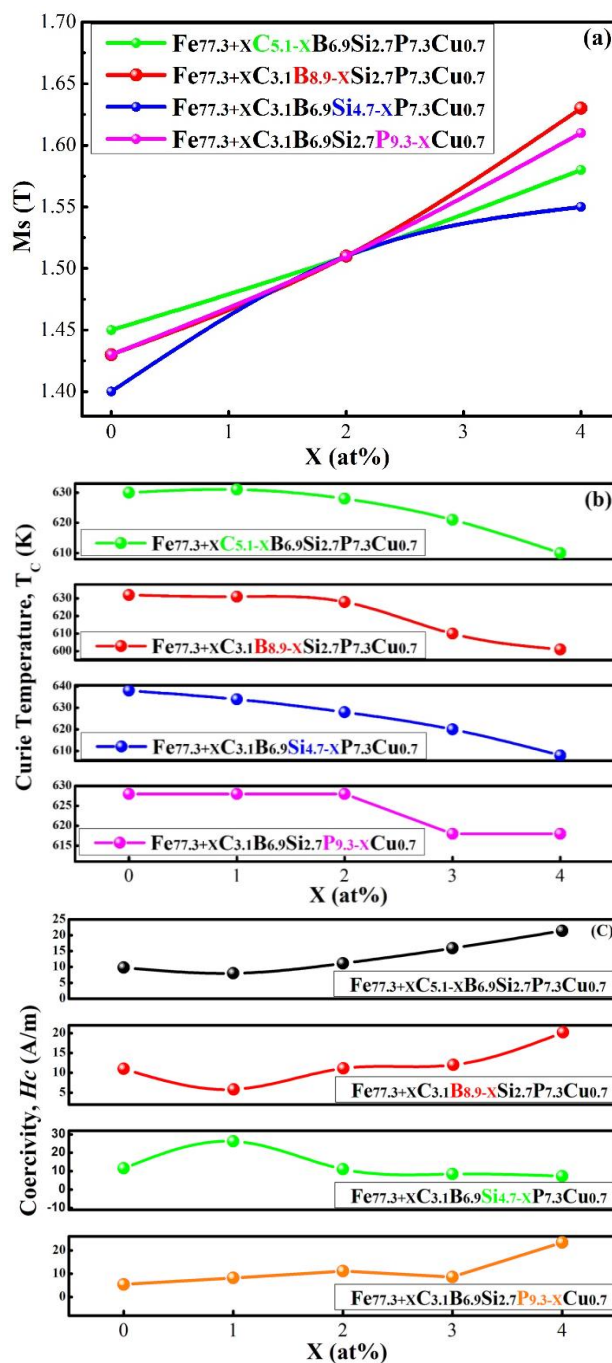


Figure 4. Changes of M_S (a), changes of Curie temperature (b), and coercivity (c) for all as-prepared FeCBSiPCu MGs as a function of content of metalloid elements.

Figure 4b shows the composition dependence of Curie temperature for all investigated FeCBSiPCu MGs. As can be seen in Figure 4b, each curve shows a decline trend, indicating that the Curie temperature declines gradually by decreasing metalloid elements. For $\text{Fe}_{77.3+x}\text{C}_{3.1}\text{B}_{8.9-x}\text{Si}_{2.7}\text{P}_{7.3}\text{Cu}_{0.7}$ ($X = 0, 1, 2, 3, 4$) alloys, the T_C shifts from 632 to 601 K, which is the maximum decrease compared with that of adjusting C, Si, and P contents. It is obvious that all curves have plateaus, especially for $\text{Fe}_{77.3+x}\text{C}_{3.1}\text{B}_{6.9}\text{Si}_{2.7}\text{P}_{9.3-x}\text{Cu}_{0.7}$ ($X = 0, 1, 2, 3, 4$) alloys; the Curie temperature even keeps as a constant value when P content is more than 7.3%, indicating that effects of metalloid elements on Curie temperature of FeCBSiPCu amorphous alloys are not remarkable if the content of metalloid elements reach to relative high value. According to molecular field theory, Curie temperature is proportional to exchange-integral constant A , which is affected by type of alloying element and distance between magnetic element. For FeCBSiPCu amorphous alloys, exchange-integral constant A is only related to Fe-Fe interaction, since there exists only one type of magnetic element Fe in FeCBSiPCu alloy system. For FeCBSiPCu amorphous alloys, $A_{\text{Fe-Fe}}$ increases, since the addition of metalloid elements such as C, B, Si, and P increases distance between two Fe atoms, which results in the increasing of Curie temperature.

Moreover, effects of metalloid elements on coercivity (H_C) of the current FeCBSiPCu MGs were also investigated. Coercivity as a function of the content of metalloid elements is shown in Figure 4c for the as-prepared Fe-based amorphous ribbons. It is of importance to point out that the lowest H_C value was achieved at the alloy with 4.1 at. % C and 7.9 at. % B, respectively. However, Si and P have different effects on the coercivity. It can be seen that for the alloy with 3.7 at. % Si, H_C is much higher than that of the rest alloys with 4.7, 2.7, 1.7, and 0.7 at. % Si. By decreasing the P content, H_C seems to be quite stable. When the P content decreases to 5.3 at. %, H_C increases sharply from 8.6 to 23.4 A/m. The influence of metalloid elements on H_C may be related to the GFA. It is generally accepted that the alloys with higher GFA have a more homogeneous structure, usually resulting in lower H_C [25]. For example, excessive or too little addition of C and B could deteriorate the GFA and lead to the higher H_C . As mentioned earlier, P has a relatively high solute limit with Fe and addition of P is beneficial for glass formation. As a result, the alloys with a high amount of P have a low coercivity value, but once the P content is lowered to 5.3 at. %, H_C sharply increases, suggesting that too little addition of P leads to the deterioration of GFA.

4. Conclusions

Partial substitution of metalloid elements with various contents of iron in the $\text{Fe}_{77.3+x}\text{C}_{5.1-x}\text{B}_{6.9}\text{Si}_{2.7}\text{P}_{7.3}\text{Cu}_{0.7}$, $\text{Fe}_{77.3+x}\text{C}_{3.1}\text{B}_{8.9-x}\text{Si}_{2.7}\text{P}_{7.3}\text{Cu}_{0.7}$, $\text{Fe}_{77.3+x}\text{C}_{3.1}\text{B}_{6.9}\text{Si}_{4.7-x}\text{P}_{7.3}\text{Cu}_{0.7}$, and $\text{Fe}_{77.3+x}\text{C}_{3.1}\text{B}_{6.9}\text{Si}_{2.7}\text{P}_{9.3-x}\text{Cu}_{0.7}$ ($X = 0, 1, 2, 3$ and 4) alloy system has been conducted, and the effects of metalloid elements on the thermal stability and soft magnetic properties of our FeCBSiPCu MGs has been investigated. The main conclusions are as follows:

1. C and B have similar influences on the crystallization behavior of investigated alloys. Increasing C or B leads to the increasing of T_{x1} , while the T_{x2} remains unchanged. Increasing Si content results in the increasing of both T_{x1} and T_{x2} . However, the increase of P content enhances T_{x1} and makes T_{x2} shift to lower temperature.
2. When the content of the metalloid elements is increased, M_S has a decreasing trend for all as-prepared ribbons. The dependence of M_S on the metalloid elements contents could be explained from the standpoint of the interactions between sp orbitals of metalloid elements and 3d electrons of Fe by increasing the content of metalloid elements.
3. For FeCBSiPCu MGs, Curie temperature declines gradually by decreasing the metalloid elements. However, the effects of metalloid elements on the Curie temperature of FeCBSiPCu MGs are not remarkable if the content of metalloid elements reaches a relatively high value.
4. The effects of metalloids on coercivity are closely related to their roles on the GFA. If their addition is beneficial for glass formation, then the coercivity value of the resultant glassy alloys will be reduced.

Acknowledgments: This research was supported by National Natural Science Foundation of China (Nos. 51671018, 51531001, 51422101, 51371003, 51271212 and 51671021), 111 Project (B07003), International S&T Cooperation Program of China (2015DFG52600), Program for Changjiang Scholars and Innovative Research Team in University of China (IRT_14R05), and the Projects of SKL-AMM-USTB (2016Z-04, 2016-09, 2016Z-16). Hongxiang Li thanks the financial support from Beijing Natural Science Foundation (No. 2142022), and Program for Excellent Talents in Beijing Municipality (No. 2013D009006000004).

Author Contributions: Zhichao Lu, Hongxiang Li, Zhifeng Lei, and Zhaoping Lu conceived and designed the experiments; Zhichao Lu performed the experiments; Zhichao Lu and Zhifeng Lei analyzed the data; Chuntao Chang and Xianzhen Wang contributed analysis tools; and Zhichao Lu wrote the paper under the guidance of Hongxiang Li and Zhaoping Lu.

Conflicts of Interest: The authors declare no conflict of interest.

References

- Inoue, A.; Zhang, T.; Takeuchi, A. Bulk amorphous alloys with high mechanical strength and good soft magnetic properties in Fe-TM-B (TM = IV–VIII group transition metal) system. *Appl. Phys. Lett.* **1997**, *71*, 464–466. [[CrossRef](#)]
- Borrego, J.M.; Conde, A.; Roth, S.; Eckert, J. Glass-forming ability and soft magnetic properties of FeCoSiAlGaPCB amorphous alloys. *J. Appl. Phys.* **2002**, *92*, 2073–2078. [[CrossRef](#)]
- Jiao, Z.B.; Li, H.X.; Gao, J.E.; Wu, Y.; Lu, Z.P. Effects of alloying elements on glass formation, mechanical and soft-magnetic properties of Fe-based metallic glasses. *Intermetallics* **2011**, *19*, 1502–1508. [[CrossRef](#)]
- Yang, X.H.; Ma, X.H.; Li, Q.; Guo, S.F. The effect of Mo on the glass forming ability, mechanical and magnetic properties of FePC ternary bulk metallic glasses. *J. Alloys Compd.* **2013**, *554*, 446–449. [[CrossRef](#)]
- Onodera, R.; Kimura, S.; Watanabe, K.; Yokoyama, Y.; Makino, A.; Koyama, K. Nucleation control for fine nano crystallization of Fe-based amorphous alloy by high-magnetic-field annealing. *J. Alloys Compd.* **2015**, *637*, 213–218. [[CrossRef](#)]
- Figuerola, E.; Lundgren, L.; Beckman, O.; Bhagat, S.M. The anomalous magnetization of amorphous metglas 2826-A. *Solid State Commun.* **1976**, *20*, 961–964. [[CrossRef](#)]
- Yoshizawa, Y.; Oguma, S.; Yamauchi, K. New Fe-based soft magnetic alloys composed of ultrafine grain structure. *J. Appl. Phys.* **1988**, *64*, 6044–6046. [[CrossRef](#)]
- Suzuki, K.; Kataoka, N.; Inoue, A.; Makino, A.; Masumoto, T. High saturation magnetization and soft magnetic properties of bcc Fe-Zr-B alloys with ultrafine grain structure. *Mater. Trans. JIM* **1990**, *31*, 743–746. [[CrossRef](#)]
- Willard, M.A.; Laughlin, D.E.; McHenry, M.E.; Thoma, D.; Sickafus, K.; Cross, J.O.; Harris, V.G. Structure and magnetic properties of $(\text{Fe}_{0.5}\text{Co}_{0.5})_{88}\text{Zr}_7\text{B}_4\text{Cu}_1$ nanocrystalline alloys. *J. Appl. Phys.* **1998**, *84*, 6773–6777. [[CrossRef](#)]
- Takenaka, K.; Nishiyama, N.; Setyawan, A.D.; Sharma, P.; Makino, A. Performance of a prototype power transformer constructed by nanocrystalline Fe-Co-Si-B-P-Cu soft magnetic alloys. *J. Appl. Phys.* **2015**, *117*, 17D519. [[CrossRef](#)]
- Hasegawa, R. Applications of amorphous magnetic alloys in electronic devices. *J. Non-Cryst. Solids* **2001**, *287*, 405–412. [[CrossRef](#)]
- Matsumoto, H.; Urata, A.; Yamada, Y.; Inoue, A. FePBNbCr soft-magnetic glassy alloys with low loss characteristics for inductor cores. *J. Alloys Compd.* **2010**, *504*, S139–S141. [[CrossRef](#)]
- Nishiyama, N.; Tanimoto, K.; Makino, A. Outstanding efficiency in energy conversion for electric motors constructed by nanocrystalline soft magnetic alloy “NANOMET[®]” cores. *AIP Adv.* **2016**, *6*, 055925. [[CrossRef](#)]
- Lei, C.; Lei, J.; Yang, Z.; Zhou, Y. Improved micro fluxgate sensor with double-layer Fe-based amorphous core. *Microsyst. Technol.* **2013**, *19*, 167–172. [[CrossRef](#)]
- Matsumoto, H.; Urata, A.; Yamada, Y.; Ioune, A. Novel FePBNbCr glassy alloys “SENNTIX” with good soft-magnetic properties for high efficiency commercial inductor cores. *J. Alloys Compd.* **2011**, *509*, S193–S196. [[CrossRef](#)]
- Sun, D.S.; Hong, S.M.; Jin, H.M.; Jin, L.; Kim, C.G.; Kim, C.O. Effect of P addition on microstructure and soft magnetic properties of $\text{Fe}_{73.5-x}\text{Nb}_3\text{Cu}_1\text{P}_x\text{Si}_{13.5}\text{B}_9$ alloys. *J. Magn. Magn. Mater.* **2006**, *304*, e198–e200. [[CrossRef](#)]

17. Cui, L.Y.; Men, H.; Makino, A.; Kubota, T.; Yubuta, K.; Qi, M. Effect of Cu and P on the crystallization behavior of Fe-rich hetero-amorphous FeSiB alloy. *Mater. Trans.* **2009**, *50*, 2515–2520. [[CrossRef](#)]
18. Mizushima, T.; Makino, A.; Inoue, A. Influence of Si addition on thermal stability and soft magnetic properties for Fe–Al–Ga–P–C–B glassy alloys. *J. Appl. Phys.* **1998**, *83*, 6329–6331. [[CrossRef](#)]
19. Chen, F.G.; Wang, Y.G. Investigation of glass forming ability, thermal stability and soft magnetic properties of melt-spun $\text{Fe}_{83}\text{P}_{16-x}\text{Si}_x\text{Cu}_1$ ($x = 0, 1, 2, 3, 4, 5$) alloy ribbons. *J. Alloys Comps.* **2014**, *584*, 377–380. [[CrossRef](#)]
20. Suzuki, K.; Makino, A.; Kataoka, N.; Inoue, A.; Masumoto, T. High saturation magnetization and soft magnetic properties of bcc Fe–Zr–B and Fe–Zr–B–M (M = transition metal) alloys with nanoscale grain size. *Mater. Trans. JIM* **1991**, *32*, 93–102. [[CrossRef](#)]
21. Wu, Y.; Hui, X.D.; Lu, Z.P.; Liu, Z.Y.; Liang, L.; Chen, G.L. Effects of metalloid elements on the glass-forming ability of Fe-based alloys. *J. Alloys Comps.* **2009**, *467*, 187–190. [[CrossRef](#)]
22. Demetriou, M.D.; Kaltenboeck, G.; Suh, J.Y.; Garrett, G.; Floyd, M.; Crewdson, C.; Hofmann, D.C.; Kozachkov, H.; Wiest, A.; Schramm, J.P.; et al. Glassy steel optimized for glass-forming ability and toughness. *Appl. Phys. Lett.* **2009**, *95*, 041907. [[CrossRef](#)]
23. Li, H.X.; Gao, J.E.; Wu, Y.; Jiao, Z.B.; Ma, D.; Stoica, A.; Wang, X.L.; Ren, Y.; Miller, M.K.; Lu, Z.P.; et al. Enhancing glass-forming ability via frustration of nano-clustering in alloys with a high solvent content. *Sci. Rep.* **2013**, *3*, 1983. [[CrossRef](#)] [[PubMed](#)]
24. Miedema, A.R.; de Chatel, P.F.; de Boer, F.R. Cohesion in alloys—Fundamentals of a semi-empirical model. *Phys. B+C* **1980**, *100*, 1–28. [[CrossRef](#)]
25. Lee, S.; Kato, H.; Kubota, T.; Yubuta, K.; Makino, A.; Inoue, A. Excellent thermal stability and bulk glass forming ability of Fe–B–Nb–Y soft magnetic metallic glass. *Mater. Trans.* **2008**, *49*, 506–512. [[CrossRef](#)]



© 2018 by the authors. Licensee MDPI, Basel, Switzerland. This article is an open access article distributed under the terms and conditions of the Creative Commons Attribution (CC BY) license (<http://creativecommons.org/licenses/by/4.0/>).